Chapter

Synthesis and Properties of Single-Walled Carbon Nanotubes Filled with Metal Halogenides and Metallocenes

Marianna V. Kharlamova and Dominik Eder

Abstract

This chapter reviews the current status of the research on the electronic properties of single-walled carbon nanotubes (SWCNTs) filled with metal halogenides and metallocenes and growth kinetics of inner SWCNTs inside metallocene-filled nanotubes. The chapter starts with the description of the peculiarities of the synthesis of metal halogenide-filled SWCNTs, comparison of different filling methods, their advantages, disadvantages, and restrictions. Then, we comprehensively summarize, compare, and critically discuss the recent studies on the electronic properties of metal halogenide-filled SWCNTs. After that, the synthesis methods of metallocene-filled SWCNTs are described and the results of the investigation of the growth kinetics of inner SWCNTs inside the filled nanotubes are summarized. Then, the reports dedicated to the investigation of the electronic properties of metallocene-filled SWCNTs are reviewed. Finally, potentials for future research, development, and application of filled SWCNTs are highlighted.

Keywords: single-walled carbon nanotube, metal halogenide, metallocene, electronic properties, growth kinetics, optical absorption spectroscopy, Raman spectroscopy, X-ray photoelectron spectroscopy

1. Introduction

Carbon nanotube, a one-dimensional allotropic modification of carbon with sp^2-hybridization of atoms, can be represented as rolled-up graphene sheets. Depending on the number of graphene layers, their structure is classified into multi-, double- (DWCNTs), and single-walled nanotubes (SWCNTs). Thanks to their unique physical and chemical properties, SWCNTs can find applications in different fields, including next-generation nanoelectronic devices [1]. The electronic properties of SWCNTs depend on their atomic structures. Due to the lack of methodology and control, nanotubes produced via industrial synthesis methods, i.e., arc-discharge, laser ablation, and chemical vapor deposition (CVD), typically exhibit varying and mixed properties, thus limiting their applicability. Despite progress on synthesis [2–6] and sorting of SWCNTs [7–11] with defined atomic structures, new methods are required that allow controllable modification of the electronic properties of SWCNTs.

Recent research has been aimed at the modification of the electronic properties of SWCNTs by the covalent and noncovalent modification of their outer surface, substitution of carbon atoms by foreign atoms, intercalation of the bundles, and filling of the channels of nanotubes [12, 13]. The latter method is especially promising, because a variety of substances with different properties can be encapsulated inside SWCNTs. The filling of SWCNTs with fullerene C_{60} [14] and $RuCl_3$ [15] was firstly performed in 1998 and since then the topic has attracted increasing attention. SWCNTs were filled with different simple elemental substances, metals [16–22] and nonmetals [17, 23], chemical compounds, metal halogenides [24–29], metal chalcogenides [30–34] and metal oxides [35, 36] as well as molecules, fullerenes and their derivatives [37–41] and metallocenes [42, 43].

Metal halogenides are the largest group of introduced inorganic substances. Depending on the metal cation and halogen anion, they are semiconductors or insulators with different work functions. The filling of SWCNTs with these salts opens the way to stable doping of nanotubes and tailoring their doping level. This triggered extensive studies on the electronic properties of metal halogenide-filled SWCNTs.

Metallocenes are another popular group of encapsulated substances. In 2008, it was shown that the high vacuum annealing of metallocene-filled SWCNTs leads to the formation of inner carbonaceous tubes [44]. In this case, metallocene molecules served as carbon and catalyst source at the same time. In contrast to the typical CVD growth of nanotubes, where the growth process stops after tens of minutes due to the deactivation of catalyst, the growth inside metallocene-filled SWCNTs was considerably slower and could last up to tens of hours until the carbon source was consumed. This enabled not only a more in-depth investigation of the growth process of nanotubes, but also of their electronic properties, which continuously evolved by filling and annealing upon chemical transformation of metallocenes. Consequently, this has attracted considerable interest in the field.

This chapter reviews the current status of the research on the electronic properties of SWCNTs filled with metal halogenides and metallocenes and growth kinetics of SWCNTs inside metallocene-filled nanotubes. The first part of the chapter focuses on the synthesis and electronic properties of SWCNTs filled with metal halogenides. We review and compare the results of the studies on the electronic properties of the filled SWCNTs by state-of-the-art spectroscopic methods such as optical absorption spectroscopy (OAS), Raman spectroscopy, and X-ray photoelectron spectroscopy (XPS). In the second part of the chapter, the results of the investigation of the growth kinetics of inner SWCNTs inside metallocene-filled nanotubes by *in situ* Raman spectroscopy and the electronic properties of the filled nanotubes by XPS and ultraviolet photoelectron spectroscopy (UPS) are summarized.

2. SWCNTs filled with metal halogenides

2.1 Synthesis of metal halogenide-filled SWCNTs

Metal halogenides were encapsulated inside SWCNTs by several methods. Among them are the gas phase and liquid phase approaches. The latter includes the solution and melt techniques.

The gas phase approach implies the encapsulation of a substance in a gas state inside SWCNTs. In the filling process, SWCNTs and substances are heated up to the temperature that is higher than the boiling or sublimation point of the substance. During dwelling at the synthesis temperature, the vapor of the substance condenses

and diffuses inside SWCNTs. Then, the system is cooled, which leads to the crystallization of the substance. The advantages of this method are that it is rather simple, and it allows obtaining high filling ratios of nanotubes. However, it has several restrictions. Firstly, the maximal boiling or sublimation point of substances cannot exceed 1000–1200°C, because at higher temperatures the destruction of nanotubes occurs. Secondly, there should be no decomposition of the substance during the evaporation or sublimation process. Thirdly, the substance should have a high vapor pressure at synthesis temperature [13]. These restrictions limit the list of substances that can be encapsulated inside SWCNTs by this approach.

The list of introduced substances can be widened by the use of the liquid phase approach. The parameters of the filling process can be broadly varied. This approach is the most popular filling technique of nanotubes.

The solution method implies the filling of SWCNTs with a chosen substance dissolved in a solvent. During the filling process, several parameters are important. For the successful filling, the solubility of the substance in the solvent should be high, whereas the surface tension coefficient of the solution and its viscosity should be low. The choice of appropriate solvents allows encapsulating different substances inside SWCNTs. However, the solution method has several disadvantages. The first of them is the contamination of filled SWCNTs with solvent molecules. This can be critical for further characterizations of filled SWCNTs. The second is low filling ratios of SWCNTs, which usually do not exceed 30%. The third is inhomogeneous morphology of introduced substances inside SWCNTs [13].

These disadvantages are absent in the melt method. This method implies the filling of SWCNTs with molten salt. In a typical experiment, opened SWCNTs are mixed with an excessive amount of salt in quartz ampoules. The ampoules are evacuated, sealed, and heated up to a temperature above the melting point of the salt. The liquid salt is pulled inside SWCNTs by capillary forces. After dwelling at high temperature for some time, the SWCNTs are saturated with filling ratios up to 90%. The final cooling rate is a way to control the crystallinity of the solidified salt inside SWCNTs. Very low cooling rates are required for obtaining one-dimensional nanocrystals. Several parameters are important for the successful filling. Firstly, the melting temperature of the salt should not exceed 1000–1200°C, because at high temperatures, the nanotubes start to degrade. Secondly, the surface tension coefficient of the melt of the salt and its viscosity should be low enough [13].

The melt method is the most popular method of the filling of SWCNTs with metal halogenides. It was applied for the filling of nanotubes in all papers dedicated to the investigation of the electronic properties of metal halogenide-filled SWCNTs.

2.2 Electronic properties of metal halogenide-filled SWCNTs

In the literature, there are the reports on the investigation of the electronic properties of SWCNTs filled with $MnCl_2$, $MnBr_2$ [45, 46], $FeCl_2$, $FeBr_2$, FeI_2 [47], $CoBr_2$ [48], $NiCl_2$ [49], $NiBr_2$ [49, 50], CuCl [51, 52], CuBr [51], CuI [51, 53, 54], $ZnCl_2$ [55, 56], $ZnBr_2$, ZnI_2 [55], RbI, $RbAg_4I_5$ [57], AgCl [58–61], AgBr, AgI [58], $CdCl_2$ [56, 62, 63], $CdBr_2$, CdI_2 [62], SnF_2 [64], $TbCl_3$ [56, 65, 66], $TbBr_3$, TbI_3 [66], $PrCl_3$ [65, 67], $ErCl_3$ [68], $TmCl_3$ [65, 69], and $HgCl_2$ [70]. The characterization of the electronic properties of the filled SWCNTs was performed by three main techniques: OAS, Raman spectroscopy, and XPS. These three methods are complementary, and they give a comprehensive picture of the modification of the electronic properties of SWCNTs upon their filling. OAS gives information about structure-dependent optical transitions of nanotubes. Raman spectroscopy allows studying the vibronic properties of SWCNTs. XPS investigates the Fermi level shift and bonding environment in filled SWCNTs.

Figure 1 shows the typical OAS spectrum of metal halogenide-filled SWCNTs by an example of the ZnI_2-filled nanotubes in comparison with the spectrum of the pristine SWCNTs [55]. The spectrum of the pristine SWCNTs includes the characteristic peaks corresponding to optical transitions between the first (E^S_{11}) and second (E^S_{22}) van Hove singularities (vHs) in the valence and conduction band of semiconducting SWCNTs and the first vHs (E^M_{11}) of metallic nanotubes. In the spectrum of the filled SWCNTs, there is the suppression of the E^S_{11} peak, which corresponds to the canceling of the optical transitions between the first vHs of semiconducting SWCNTs. This is a result of the shift of the Fermi level of SWCNTs below the first vHs in the valence band or above the first vHs in the conduction band of semiconducting SWCNTs. Thus, the OAS data testify to the presence of the charge transfer in the filled SWCNTs; however, the direction of the charge transfer cannot be determined. The same modifications were observed in the OAS spectra of SWCNTs filled with $FeCl_2$, $FeBr_2$, FeI_2 [47], $CoBr_2$ [48], $ZnCl_2$, $ZnBr_2$ [55], AgCl, AgBr, AgI [58], $CdCl_2$, $CdBr_2$, CdI_2 [62], CuCl, CuBr, CuI [51], CuCl [52], and $TbCl_3$ [56].

Raman spectroscopy allows obtaining further information about the charge transfer in the filled SWCNTs. A Raman spectrum of SWCNTs includes two main characteristic bands: radial breathing mode (RBM), which corresponds to radial vibrations of carbon atoms, and G-band, which belongs to longitudinal and tangential vibrations of carbon atoms [71]. **Figure 2** demonstrates the RBM and G-bands of Raman spectra of $CdCl_2$-filled SWCNTs in comparison with the spectra of the pristine nanotubes acquired at seven different laser wavelengths between 458 and 785 nm [63]. It is visible that all spectra of the filled SWCNTs are significantly modified as compared to the spectra of the pristine SWCNTs. The shift and change of the relative intensity of the peaks of the RBM band, the shift of the peaks of the G-band, and the change in the profile of the G-band are observed. These modifications are common for metal halogenide-filled SWCNTs. They were reported for SWCNTs filled with $MnCl_2$, $MnBr_2$ [45, 46], $FeCl_2$, $FeBr_2$, FeI_2 [47], $CoBr_2$ [48],

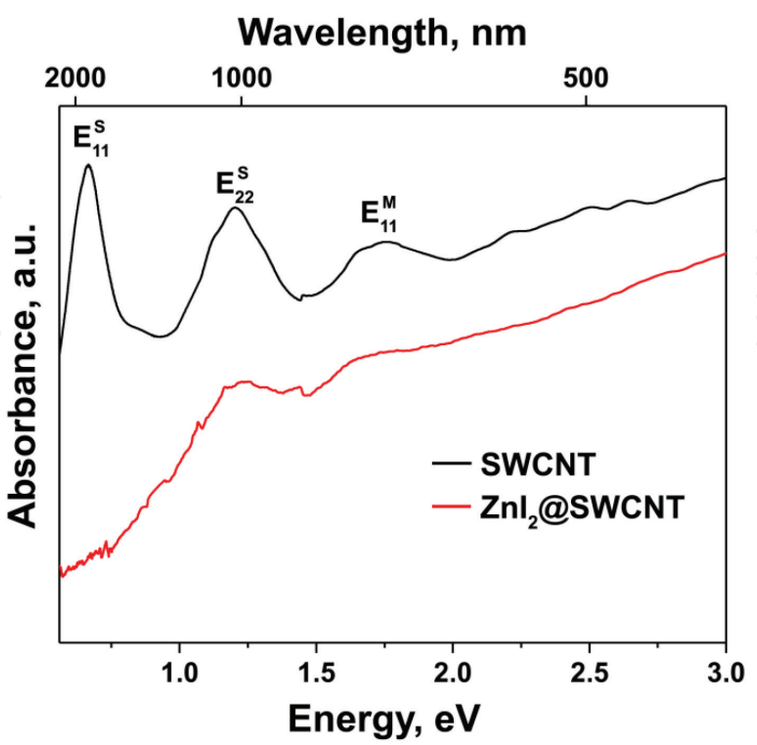

Figure 1.
The OAS spectra of the pristine and ZnI_2-filled SWCNTs. The peaks corresponding to optical transitions between the first (E^S_{11}) and second vHs (E^S_{22}) of semiconducting SWCNTs and the first vHs (E^M_{11}) of metallic SWCNTs are denoted. The data are replotted from ref. [55].

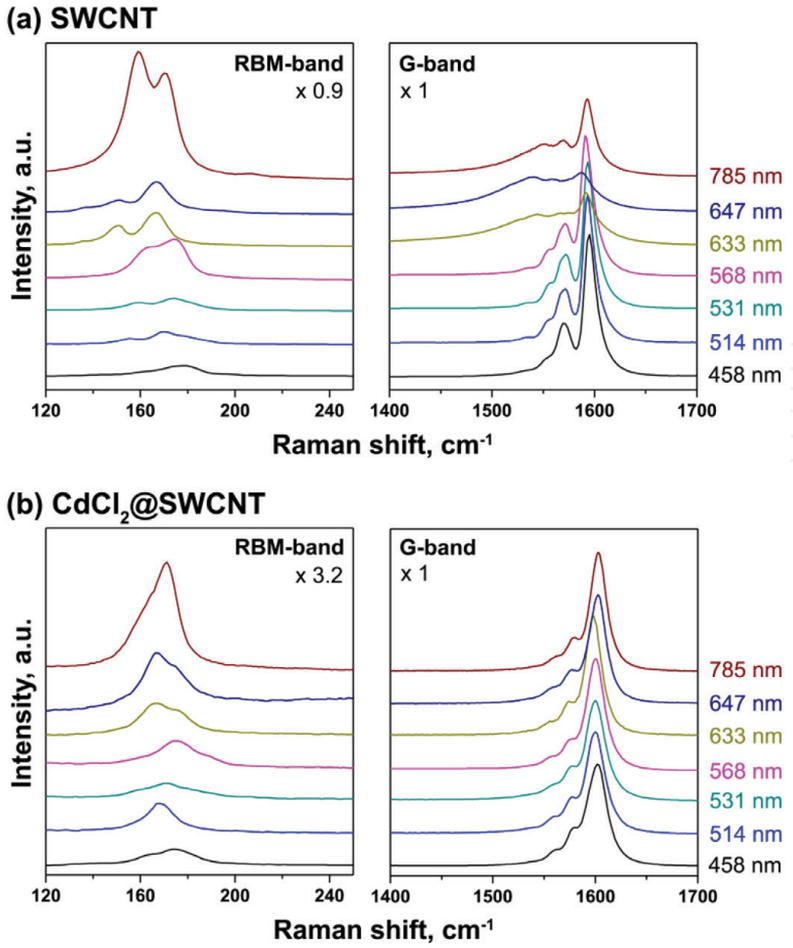

Figure 2.
The RBM and G-bands of Raman spectra of the pristine (a) and CdCl2-filled SWCNTs (b) acquired at different laser wavelengths. The spectra are normalized to the area intensity of the G-band and offset for clarity. The data are replotted from ref. [63].

$NiCl_2$, $NiBr_2$ [49], CuCl [51, 52], CuBr [51], CuI [51, 53, 54], $ZnCl_2$ [55, 56], $ZnBr_2$, ZnI_2 [55], $CdBr_2$, CdI_2 [62], SnF_2 [64], $RbAg_4I_5$ [57], $TbCl_3$ [56, 65, 66], $TbBr_3$, TbI_3 [66], $TmCl_3$ [65, 69], $PrCl_3$ [65, 67], AgCl [58–61], AgBr, AgI [58], and $HgCl_2$ [70].

The fitting of the RBM and G-bands of Raman spectra with individual components allows investigating in detail the observed modifications. **Figure 3** shows the fitting results of the spectrum of the $TbBr_3$-filled SWCNTs in comparison with the spectrum of pristine nanotubes acquired at laser wavelength of 633 nm [66]. The RBM-band of the pristine SWCNTs is fitted with two components at 156 and 172 cm^{-1}, which correspond to the nanotubes with diameters of 1.5 and 1.4 nm, respectively [72]. The G-band of the pristine SWCNTs is fitted with three components. The peak at 1540 cm^{-1} (G^-) belongs to longitudinal phonon in metallic SWCNTs, and the peaks at 1567 and 1591 cm^{-1} (G^+_{TO} and G^+_{LO}) are assigned to tangential and longitudinal phonons in semiconducting SWCNTs, respectively [73]. The RBM band of the filled SWCNTs is fitted with two components, as the spectrum of the pristine SWCNTs. However, the peak positions are shifted to 164 and 175 cm^{-1}, and also the ratio of the relative intensities of the peaks is changed from 0.32:0.68 to 0.53:0.47. These modifications are due to the changes in resonance conditions of the filled SWCNTs, which are caused by the charge transfer in the filled nanotubes. The G-band of the filled SWCNTs is fitted with three components, as the spectrum of the pristine nanotubes. However, their positions are upshifted to 1558, 1576, and 1602 cm^{-1}. This can be attributed to the p-doping of SWCNTs by the encapsulated compound. Additionally, there is the change of the profile

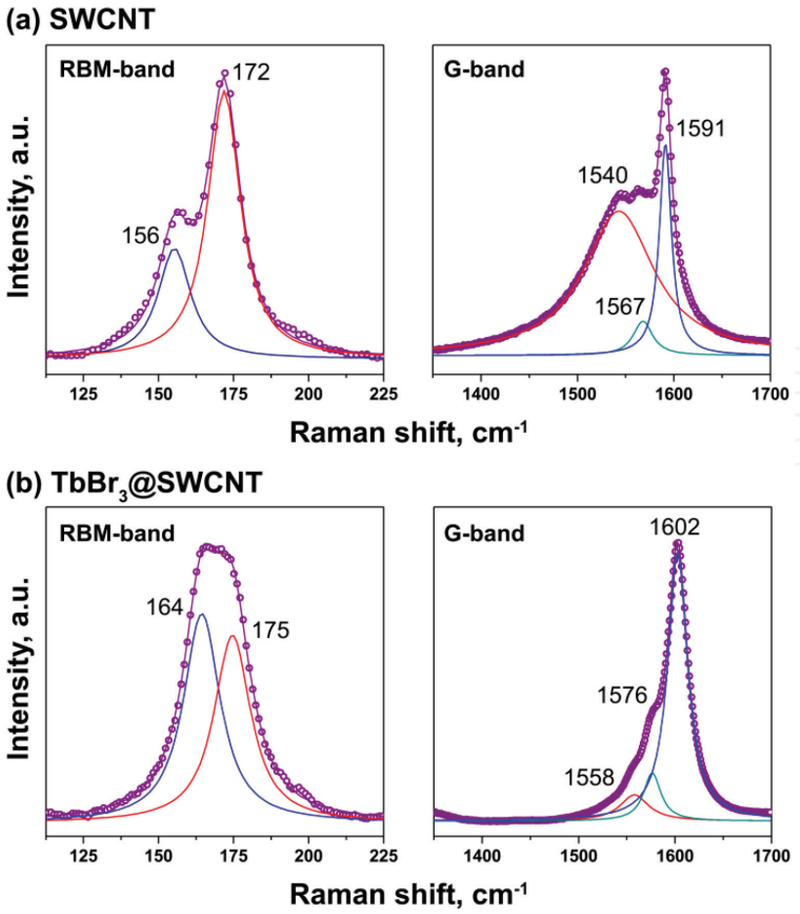

Figure 3.
The fitting of the RBM and G-bands of Raman spectra of the pristine (a) and $TbBr_3$-filled SWCNTs (b) acquired at laser wavelength of 633 nm with individual components. The peak positions are denoted. The data are replotted from ref. [66].

of the G-band of the filled SWCNTs from the Breit-Wigner-Fano shape, which is typical for metallic SWCNTs [71, 74] to the Lorentzian shape, which is a fingerprint of semiconducting SWCNTs [71, 74, 75]. This is probably a result of the filling-induced transition of metallic nanotubes into semiconducting state due to the opening of a band gap in their band structure.

Although similar modifications of Raman spectra of metal halogenide-filled SWCNTs testify to p-doping of nanotubes by the encapsulated salts, the doping level varies for different compounds. In Ref. [66], the doping level of SWCNTs by introduced $TbCl_3$, $TbBr_3$, and TbI_3 was compared. Authors analyzed the modifications of RBM and G-bands of Raman spectra of the filled SWCNTs acquired at laser wavelength of 633 nm. **Figure 4** shows the results of the analysis. In **Figure 4(a)**, the relative intensities of the RBM peaks of the pristine and filled SWCNTs are presented. In the case of the pristine SWCNTs, the second peak of the RBM band has the largest intensity and the ratio of relative intensities of two RBM peaks amounts to 0.32:0.68. In the case of the $TbCl_3$- and $TbBr_3$-filled SWCNTs, in contrast, the first peak has the largest intensity and the ratio is changed to 0.55:0.45 and 0.53:0.47, respectively. In the case of the TbI_3-filled SWCNTs, the ratio of the pristine SWCNTs (0.27:0.73) is recovered. Thus, the largest differences as compared to the pristine SWCNTs are observed for the $TbCl_3$-filled SWCNTs, and the smallest differences are observed for the TbI_3-filled nanotubes. In **Figure 4(b)**, the shift of the G-band peaks and the relative area intensity of the G^--peak of the pristine and filled SWCNTs are presented. It is visible that the largest changes as compared to the pristine SWCNTs are again observed for the $TbCl_3$-filled SWCNTs and the smallest changes are observed

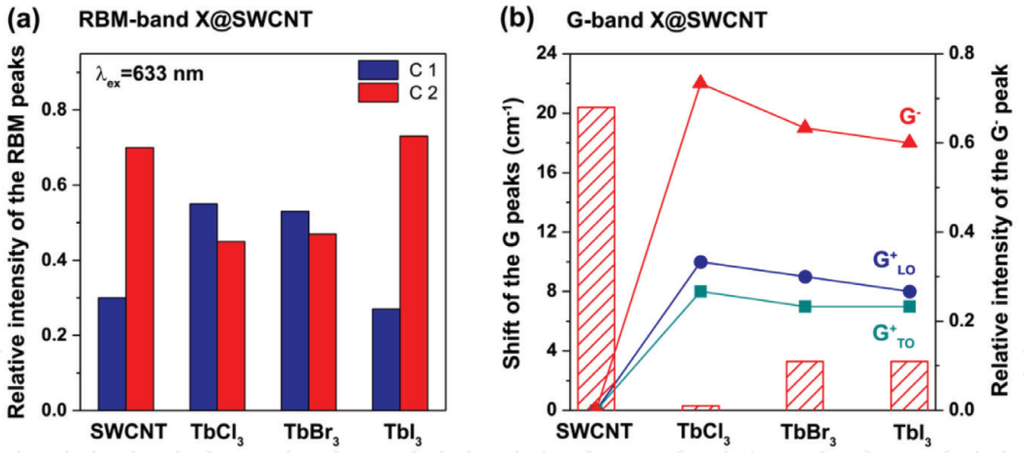

Figure 4.
The relative intensity of the RBM peaks, (a) shift of the G-band peaks and relative intensity of the G^- peak (b) in Raman spectra of the pristine SWCNTs and nanotubes filled with $TbCl_3$, $TbBr_3$, and TbI_3. The data are replotted from ref. [66].

for TbI_3-filled nanotubes. For example, the shift of the G^--peak decreases from 22 to 19 to 16 cm^{-1} in the line $TbCl_3$-$TbBr_3$-TbI_3. The relative intensity of the G^--peak decreases from 0.70 for the pristine SWCNTs to 0.01 for $TbCl_3$, 0.11 for $TbBr_3$ and 0.11 for TbI_3. On the basis of these data, the authors of Ref. [66] concluded that $TbCl_3$ causes the largest doping of SWCNTs, whereas TbI_3 results in the smallest doping.

Authors also investigated the influence of metal cation of metal halogenides on the changes of the electronic properties of SWCNTs. The above-described analysis of RBM and G-bands of Raman spectra was conducted for SWCNTs filled with $FeBr_2$, $CoBr_2$ and $NiBr_2$ [50] and $TmCl_3$, $TbCl_3$, and $PrCl_3$ [65]. It was revealed that the doping level of SWCNTs increases in the lines with $NiBr_2$-$CoBr_2$-$FeBr_2$ and $PrCl_3$-$TbCl_3$-$TmCl_3$.

Thus, Raman spectroscopy allowed revealing p-doping of SWCNTs and elucidating the differences in the doping efficiency of different metal halogenides on nanotubes. However, similar to OAS, Raman spectroscopy does not give quantitative information on the doping level of SWCNTs.

XPS spectroscopy allows quantifying the doping level of nanotubes. **Figure 5(a)** presents the typical C 1s XPS spectrum of the metal halogenide-filled SWCNTs by an example of $MnCl_2$-filled nanotubes in comparison with the spectrum of the pristine SWCNTs [46]. The spectrum of the pristine SWCNTs is a single peak

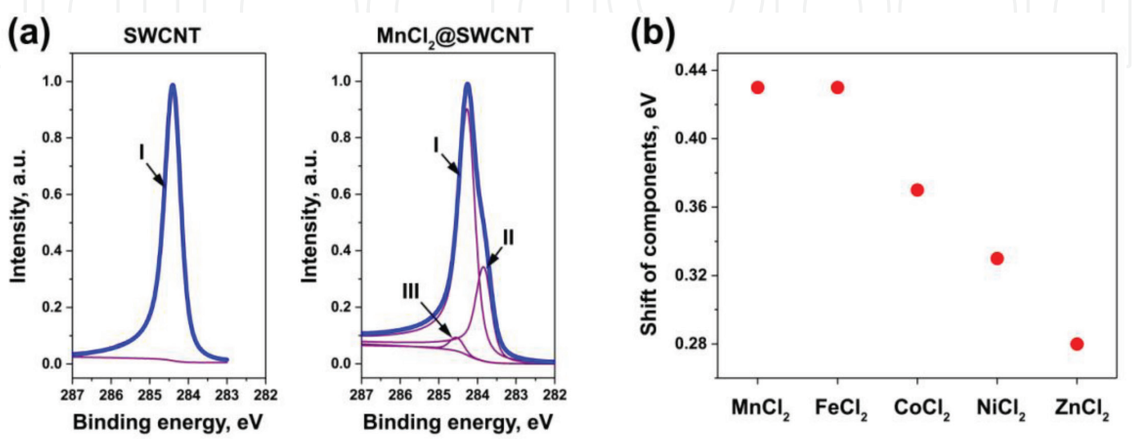

Figure 5.
(a) The C 1s XPS spectra of the pristine and $MnCl_2$-filled SWCNTs fitted with individual components. The components are denoted. The data are replotted from ref. [46]. (b) The shift of the component II relatively to the position of the component I in the C 1s XPS spectra of SWCNTs filled with $MnCl_2$, $FeCl_2$, $CoCl_2$, $NiCl_2$, and $ZnCl_2$. The data from refs. [46, 47, 49, 55] are taken into consideration for the preparation of the figure.

positioned at a binding energy of 284.38 eV. The spectrum of the filled nanotubes can be fitted with three components. The component I resembles the position and full width at half maximum of the pristine SWCNTs and it is assigned to the unfilled SWCNTs. The component II is downshifted by 0.43 eV relative to component I. This is attributed to an increase in the work function of the filled SWCNTs, which is caused by the charge transfer-induced downshift of the Fermi level of nanotubes. The origin of the component III is possibly caused by local interactions of carbon atoms of SWCNTs with atoms of the incorporated salt. Similar modifications were observed in the C 1s XPS spectra of SWCNTs filled with $MnBr_2$ [45, 46], $FeCl_2$, $FeBr_2$, FeI_2 [47], $CoBr_2$ [48], $NiCl_2$, $NiBr_2$ [49], $ZnCl_2$ [55, 56], $ZnBr_2$, ZnI_2 [55], $CdCl_2$ [56, 62], $CdBr_2$, CdI_2 [62], AgCl, AgBr, AgI [58], CuCl, CuBr, CuI [51], $RbAg_4I_5$ [57], $TbCl_3$ [56], $TmCl_3$ [69], and $PrCl_3$ [67]. The measured shifts of the component II relative to the component I amounted to 0.3–0.4 eV, and they were attributed to p-doping of SWCNTs by the encapsulated compounds.

Figure 5(b) compares the shifts of the component II relative to component I for SWCNTs filled with $MnCl_2$, $FeCl_2$, $CoCl_2$, $NiCl_2$, and $ZnCl_2$ [46, 47, 49, 55]. It is visible that the shift decreases in the line with $MnCl_2$-$FeCl_2$-$CoCl_2$-$NiCl_2$-$ZnCl_2$. This may testify that the doping level of SWCNTs decreases in this line. This conclusion is in agreement with the above-discussed data of Raman spectroscopy, which showed that among bromides of Fe, Co, and Ni, the doping efficiency decreased in the line with $FeBr_2$-$CoBr_2$-$NiBr_2$.

Thus, a comprehensive characterization of the electronic properties of SWCNTs filled with halogenides of 3d-, 4d-, and 4f-metals by OAS, Raman spectroscopy, and XPS showed that they lead to p-doping of SWCNTs accompanied by the downshift of their Fermi level. The differences in the doping level for different metal halogenides depending on metal cation and halogen anion were revealed.

3. SWCNTs filled with metallocenes

3.1 Synthesis of metallocene-filled SWCNTs

Metallocene molecules are not stable at high temperatures. The powders of substances decompose and could not be melted. At the same time, they sublime in vacuum at low temperatures. Taking into consideration this fact, researchers introduced metallocenes inside the nanotubes by the gas phase method. In a typical experiment, the SWCNTs were mixed with the powder of substances, sealed in an ampoule under vacuum, and heated at low temperatures (50–200°C) during several days. This method allowed filling SWCNTs with ferrocene [44, 76–86], cobaltocene [87, 88], nickelocene [89–92], and cerocene [93, 94]. It should be noted that ferrocene was also incorporated inside SWCNTs by the liquid phase method using its solution in acetone [95].

3.2 Temperature-dependent inner tube growth inside metallocene-filled SWCNTs

The temperature-dependent inner tube growth inside furnace- or laser-annealed ferrocene- [76, 77, 79], cobaltocene- [87], and nickelocene-filled SWCNTs [89, 90] was investigated by Raman spectroscopy. Authors traced modifications of Raman spectra of the filled SWCNTs that occurred at increasing annealing temperature or laser power at fixed annealing time. **Figure 6** presents the example of the investigation of the inner tube growth inside nickelocene-filled SWCNTs [89]. **Figure 6(a)** shows the RBM-bands of Raman spectra of the pristine, filled SWCNTs, and the

samples annealed at temperatures between 400 and 1200°C for 2 h acquired at laser wavelength of 633 nm. The RBM-band of the pristine SWCNTs includes the peak at frequencies ranging from 125 to 160 cm^{-1}. This peak is shifted by 4 cm^{-1} after filling with nickelocene, which is usually observed for molecule-filled SWCNTs. Annealing at 400°C and higher temperatures results in an appearance of new peaks centered at 212, 216, and 253 cm^{-1}. These peaks belong to inner nanotubes with chiralities of (12,3), (13,1) and (11,1) and diameters of 1.081, 1.064, and 0.909 nm, respectively. The gradual increase in annealing temperature leads to an increase of the intensity of the peaks. **Figure 6(b)** demonstrates the dependence of the relative intensity of the peak of the (12,3) and (13,1) inner tubes on annealing temperature. It is visible that the intensity increases at temperatures ranging from 400 to 700°C. It saturates at 700°C and stays almost unchanged at higher annealing temperatures. Thus, inner tubes grow in the temperature range between 400 and 700°C.

Authors of Ref. [90] compared the growth temperatures of eight different inner tubes with chiralities of (7,5), (8,4), (7,6), (10,3), (12,3), (11,5), (14,2), (12,6) inside nickelocene-filled SWCNTs. They evaluated the growth temperature as the temperature at which the intensity of the RBM peak of the inner tube reaches the half of its maximum. **Figure 7(a)** and **(b)** shows the dependences of the growth temperature of the inner tubes on their diameter and chiral angle. It is visible that the growth temperature increases with increasing tube diameter, but it does not depend on their chiral angle. The same trend was observed for inner tubes grown inside ferrocene- [77] and cobaltocene-filled SWCNTs [87].

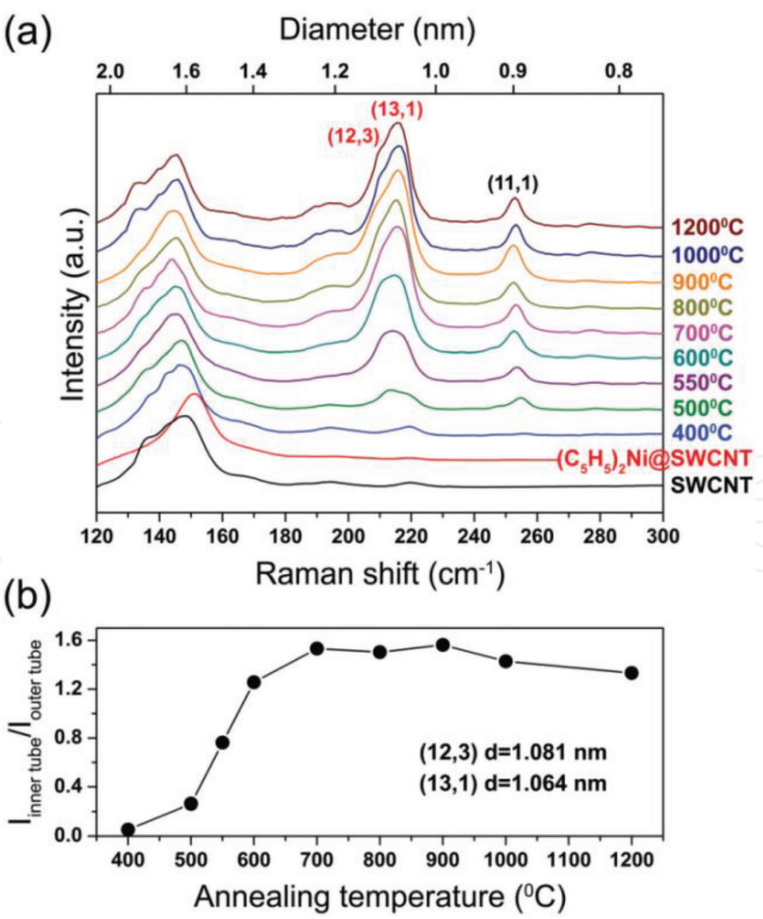

Figure 6.
(a) The RBM-band of Raman spectra of the pristine, nickelocene-filled SWCNTs, and the samples annealed at temperatures between 400 and 1200°C for 2 h acquired at laser wavelength of 633 nm. The peaks corresponding to the inner nanotubes with chiralities of (12,3), (13,1), and (11,1) are denoted. (b) The relative area intensity of the RBM peak of the inner tubes with chiralities of (12,3) and (13,1) plotted versus annealing temperature [89]—Published by The Royal Society of Chemistry.

3.3 Growth kinetics of inner tubes inside metallocene-filled SWCNTs

A detailed investigation of the growth kinetics of inner tubes inside in situ annealed nickelocene- [91], cobaltocene- [88], and ferrocene-filled SWCNTs [78] was conducted by Raman spectroscopy. Authors traced modifications of Raman spectra of the filled SWCNTs at increasing annealing time at a fixed temperature. **Figure 8** presents the example of the investigation of the growth kinetics of inner tubes inside nickelocene-filled SWCNTs [91]. **Figure 8a** shows the RBM-bands of Raman spectra of the pristine, filled SWCNTs, and the samples annealed at 540°C for the time periods between 2 and 4094 min acquired at laser wavelength of 568 nm. The spectrum of the pristine SWCNTs includes two peaks positioned at frequencies ranging from 125 to 185 cm^{-1}. They are shifted by 10 cm^{-1} for the filled SWCNTs. The spectra of the annealed samples include new peaks of inner tubes at frequencies between 205 and 295 cm^{-1}. The intensity of the peaks increases with increasing annealing time. **Figure 8(b)** demonstrates the dependence of the normalized area intensity of the RBM peaks on annealing time (growth curves) for nine different inner tubes with chiralities of (8,8), (12,3), (13,1), (9,6), (10,4), (11,2), (11,1), (9,3), and (9,2). It is visible that after an increase in the first minutes of annealing the intensity saturates and stays uncharged at further annealing. The growth curves differ for different inner tubes. The time period required for the saturation of the intensity gradually decreases with decreasing tube diameter.

The observed growth curves of inner tubes do not follow a self-exhausting growth model that was reported for the SWCNT growth in the chemical vapor deposition method. Authors of Ref. [91] modeled the growth of inner tubes by a new mathematical model including two growth rates α and β. The dependence of the amount of carbon in the form of grown inner tubes on time is expressed by the formula:

$$C(t) = A_0\left(1 - \chi e^{-\alpha t} - (1 - \chi) e^{-\beta t}\right),$$

where A_0 is the initial amount of carbon that can be transformed to inner tubes (at t = 0), α is the rate that determines the fast growth of inner tubes at the beginning, β is the rate that determines the slow growth over longer annealing hours, and χ describes which parts of carbon processed with rates α and β.

The fitting of the experimental growth curves with this model (**Figure 8(b)**) allowed calculating two rates α and β of the growth of inner tubes. **Figure 9** summarizes the calculated rates of the growth of inner tubes with chiralities of (8,8), (12,3), (13,1), (9,6), (10,4), (11,2), (11,1), (9,3), and (9,2) inside

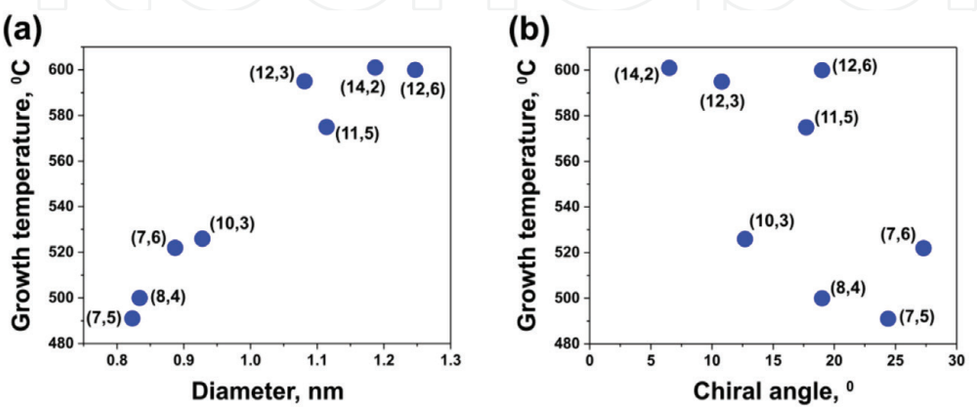

Figure 7.
The dependence of the growth temperature of inner tubes inside nickelocene-filled SWCNTs on their diameter (a) and chiral angle (b). The chirality of nanotube is indicated near the corresponding circle. The data are replotted from ref. [90].

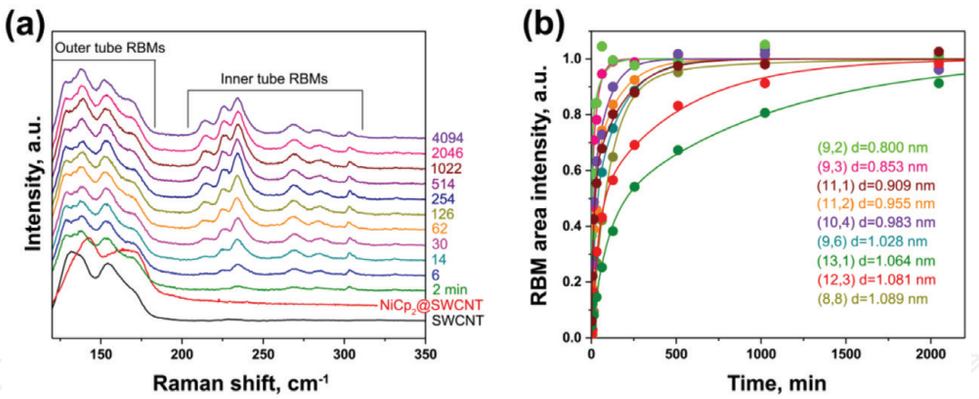

Figure 8.
(a) The RBM-band of Raman spectra of the pristine, nickelocene-filled SWCNTs, and the samples annealed at 540°C for time periods between 2 and 4094 min acquired at laser wavelength of 568 nm. The inner and outer tube RBMs are denoted. (b) The normalized RBM area intensity of inner tube peaks plotted versus annealing time. The data are replotted from Ref. [91].

nickelocene-filled SWCNTs at different annealing temperatures [91]. Two trends are observed in these plots. Firstly, the growth rates α and β increase with increasing annealing temperature from 480 to 600°C, which is caused by the fact that the inner tube growth is a thermally activated process. Secondly, they increase with decreasing the inner tube diameter from 1.1 to 0.8 nm. This can be explained by the increased catalytic activity of smaller-diameter nanoparticles [91]. It should be noted that the growth rates α and β do not depend on the chiral angle of inner tubes. The same trends were observed for the inner tube growth inside cobaltocene-filled SWCNTs [88].

Using logarithmic plots of the growth rates, two activation energies E_α and E_β of the growth of inner tubes inside nickelocene- [91] and cobaltocene-filled SWCNTs [88] were calculated. The values of E_α and E_β for the inner tubes with chiralities of (8,8), (12,3), (13,1), (9,6), (10,4), (11,2), (11,1), (9,3), and (9,2) amounted to 2.02–2.57 and 1.23–1.84 eV in the case of nickelocene, and 1.72–2.71 and 0.46–1.59 eV in the case of cobaltocene, respectively. Two activation energies were attributed to the energy barriers for solid-state diffusion of carbon through carbidic and purely metallic catalytic nanoparticles. **Figure 10(a)** and **(b)** presents the dependences of the activation energies of the inner tube growth inside nickelocene-filled SWCNTs on the tube diameter and chiral angle [91]. It is visible that the activation energy E_α gradually decreases with decreasing the tube diameter, which was explained by the size effect, whereas E_β does not show a clear dependence. Both activation energies do not seem to depend on chiral angle of inner tubes.

The identical growth mechanism of inner tubes inside nickelocene- and cobaltocene-filled SWCNTs allowed authors of Ref. [88] to compare the rates and activation energies of the growth on Ni and Co catalysts. The activation energies E_α of the inner tube growth on two catalysts were in line with each other, whereas E_β values were larger for Ni catalyst. This was in agreement with the slightly different activation energies reported for solid-state carbon diffusion through face-centered cubic nickel and cobalt with hexagonal close packed lattice. Major differences were observed for the growth rates of inner tubes on Ni and Co catalysts at a given temperature. The temperature at which inner tubes started to grow differed by 60°C. It amounted to 480°C for Ni and 540°C for Co catalyst. As a result, at a given temperature, the growth rates of inner tubes on Ni catalyst were significantly larger than those on Co catalyst. This was explained by different thermal stabilities of nickel and cobalt carbides, and different diffusion coefficients of carbon in the two metals.

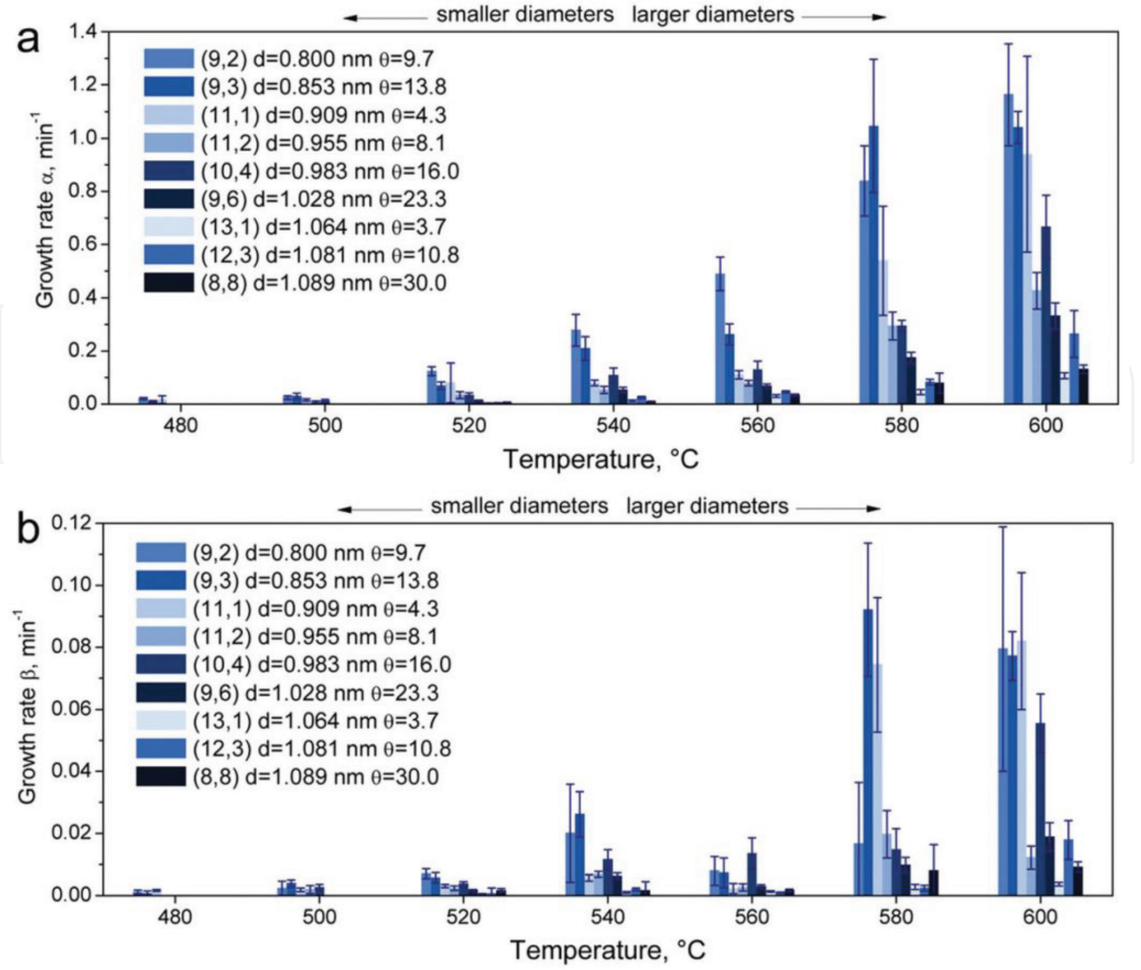

Figure 9.
The column bar diagrams showing the rates α (a) and β (b) of the growth of inner nanotubes inside nickelocene-filled SWCNTs at different annealing temperatures. At every annealing temperature, the column bar of the smallest diameter tube is shown at the leftmost side, and the largest diameter tube—at the rightmost side. The color of column bars reflects the chiral angle of inner tubes: the lightest color shade of blue corresponds to the smallest chiral angle and the darkest—to the largest chiral angle [91]—Published by The Royal Society of Chemistry.

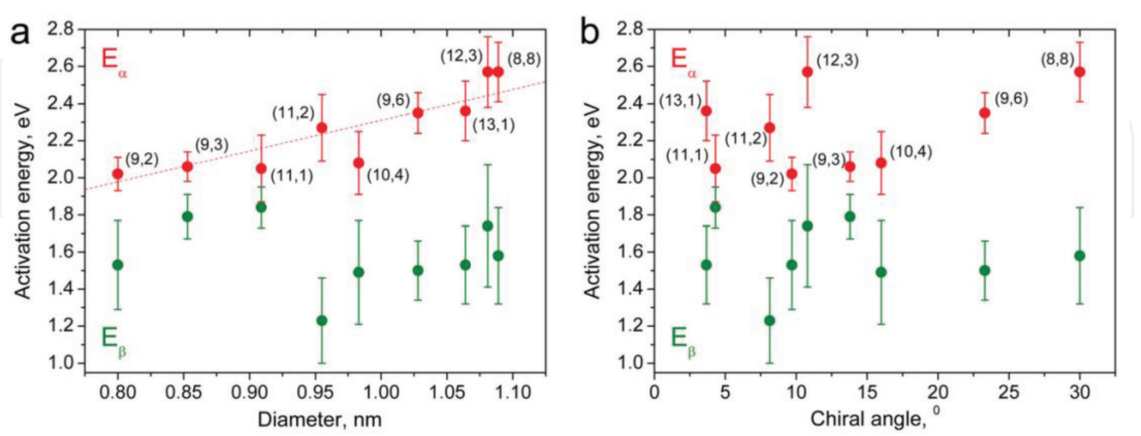

Figure 10.
The activation energies E_α and E_β of the growth of inner nanotubes inside nickelocene-filled SWCNTs plotted versus the tube diameter (a) and chiral angle (b). The chirality of nanotubes is indicated near the corresponding circle [91]—Published by The Royal Society of Chemistry.

3.4 Electronic properties of metallocene-filled SWCNTs

The electronic properties of SWCNTs filled with ferrocene [82], nickelocene [89, 90, 92], and cerocene [93, 94] were studied by XPS and UPS. It was shown

that the encapsulated metallocenes cause n-doping of SWCNTs. Authors of Refs. [82, 89, 90, 92, 93] investigated the modification of the electronic properties of the filled SWCNTs upon annealing. **Figure 11(a)** shows the UPS spectra of the pristine, nickelocene-filled SWCNTs, and the samples annealed at temperatures between 250 and 1200°C for 2 h [89]. The spectrum of the pristine SWCNTs includes π- and σ-peaks positioned at binding energies of 3.18 and 8.0 eV, respectively. The spectrum of nickelocene-filled SWCNTs demonstrates the shift of the π-peak by 0.07 eV toward higher binding energies. The annealing of the filled SWCNTs at 250°C leads to a further upshift of the π-peak by 0.18 eV. At increasing annealing temperature, the π-peak gradually shifts toward lower binding energies and reaches the position of the pristine SWCNTs at 600°C. At further increase in annealing temperature, the π-peak downshifts and reaches the maximal shift of 0.18 eV at 1200°C. The change in the position of the π-peak testifies about the change in the doping level of SWCNTs upon annealing. Authors of Ref. [89] suggested that this change is caused by three processes: (i) the chemical modification of the filler of SWCNTs, (ii) the inner tube growth, and (iii) the evaporation of the filler. The annealing of the nickelocene-filled SWCNTs leads to the formation of nickel carbide that causes the largest n-doping level of SWCNTs. As it was discussed above, at 400°C, the inner

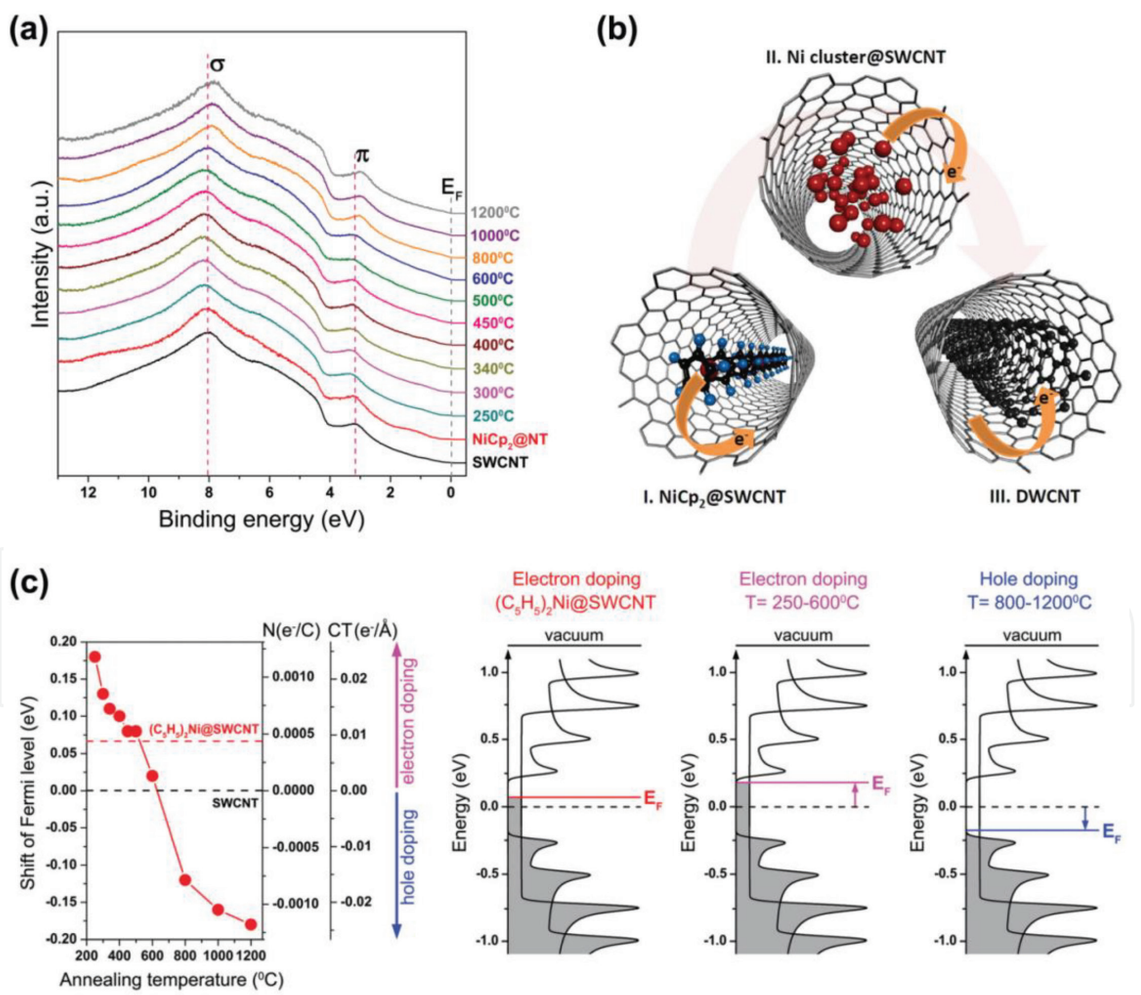

Figure 11.
(a) The UPS spectra of the pristine, nickelocene-filled SWCNTs, and the samples annealed at temperatures between 250 and 1200°C for 2 h. The π- and σ-peaks and the Fermi level (E_F) are denoted. (b) The schematics showing the charge transfer in nickelocene-filled SWCNTs (I), Ni cluster-filled SWCNTs (II) and DWCNTs (III). (c) The shift of the Fermi level, number of transferred electrons per carbon atom of SWCNTs ($N(e^-/C)$) and charge transfer density per nanotube length ($CT(e^-/Å)$) plotted versus annealing temperature as well as the schematics of electron and hole doping in the filled and annealed samples [89]—Published by The Royal Society of Chemistry.

tube growth starts and nickel carbide decomposes to pure nickel. This leads to the formation of nickel-filled DWCNTs. In DWCNTs, there is p-doping of outer tube by inner tube, which leads to decreasing the n-type doping. At high temperatures, nickel evaporates, and it leaves empty DWCNTs. It explains the largest p-doping of nanotubes at 1200°C. **Figure 11(b)** presents the schematics showing the charge transfer in the filled SWCNTs and annealed samples. **Figure 11(c)** demonstrates the shift of the Fermi level, calculated number of transferred electrons per carbon atom of SWCNTs (N(e^-/C)) and charge transfer density per nanotube length (CT(e^-/Å)) plotted versus annealing temperature as well as the schematics of n- and p-doping in the filled and annealed samples.

Similar thermally induced modifications of the electronic properties were reported for metallicity-mixed SWCNTs filled with ferrocene [82] and cerocene [93] as well as for metallicity-sorted semiconducting SWCNTs filled with nickelocene [92].

4. Conclusions and outlook

The literature survey conducted in this chapter shows that filling with metal halogenides leads to p-doping of SWCNTs. The doping level strongly depends on the metal cation and halogen anion. In contrast, filling with metallocenes leads to n-doping of SWCNTs. The high vacuum annealing of metallocene-filled SWCNTs further results in the growth of inner tubes with altered electronic properties. The growth kinetics of inner SWCNTs is characterized with two growth rates and activation energies. They show the dependence on the tube diameter and metal catalyst type.

The trends revealed in this chapter based on filling-induced modifications of the electronic properties of SWCNTs, and the growth kinetics of SWCNTs will provide the foundation for the dedicated preparation of SWCNTs with defined properties that are required for advanced applications.

However, despite the remarkable progress in the filling of SWCNTs and the controllable modification of their properties, there remain challenges that currently limit the applicability of filled SWCNTs in devices. The first issue is the scale of synthesis. Indeed, the filling routes of SWCNTs on a laboratory scale are well developed. However, for the implementation of filled SWCNTs in devices, it is crucial to up-scale the filling methods. The second issue is the filling yield. The filling is often not uniform throughout the entire sample batch. The optimization of reliable and reproducible strategies of filling of SWCNTs is necessary for application testing and the fabrication of real devices based on filled SWCNTs. The third issue involves the crystallinity of encapsulated substances. Although in many cases, well-ordered one-dimensional nanocrystals inside SWCNTs have been achieved by the melt method, there remains a lack of uniformity regarding the crystallization degree and phase composition of the filling compound. Therefore, a better understanding of the filling mechanism of SWCNTs is key to address these issues. It is important to further investigate the correlation between the synthesis parameters and the filling material. This should enable a considerable improvement on the filling ratio, crystallinity and uniformity, and thus will open new avenues for large-scale synthesis of filled SWCNTs.

Acknowledgements

This work was funded by the Deutsche Forschungsgemeinschaft (DFG ED 221/3-1).

DOI: http://dx.doi.org/10.5772/intechopen.85062

Author details

Marianna V. Kharlamova* and Dominik Eder
Institute of Materials Chemistry, Vienna University of Technology, Vienna, Austria

*Address all correspondence to: mv.kharlamova@gmail.com

References

[1] Endo M, Strano MS, Ajayan PM. Potential applications of carbon nanotubes. In: Jorio A, Dresselhaus G, Dresselhaus MS, editors. Carbon Nanotubes: Topics in Applied Physics. Berlin: Springer-Verlag; 2008. pp. 13-61. DOI: 10.1007/978-3-540-72865-8_2

[2] Chiang WH, Sankaran RM. Linking catalyst composition to chirality distributions of as-grown single-walled carbon nanotubes by tuning Ni_xFe_{1-x} nanoparticles. Nature Materials. 2009;**8**(11):882-886. DOI: 10.1038/nmat2531

[3] Ghorannevis Z, Kato T, Kaneko T, Hatakeyama R. Narrow-chirality distributed single-walled carbon nanotube growth from nonmagnetic catalyst. Journal of the American Chemical Society. 2010;**132**(28): 9570-9572. DOI: 10.1021/ja103362j

[4] He MS, Jiang H, Liu BL, Fedotov PV, Chernov AI, Obraztsova ED, et al. Chiral-selective growth of single-walled carbon nanotubes on lattice-mismatched epitaxial cobalt nanoparticles. Scientific Reports. 2013;**3**:1460. DOI: 10.1038/srep01460

[5] Yang F, Wang X, Zhang DQ, Yang J, Luo D, Xu ZW, et al. Chirality-specific growth of single-walled carbon nanotubes on solid alloy catalysts. Nature. 2014;**510**(7506):522-524. DOI: 10.1038/nature13434

[6] Zhao QC, Xu ZW, Hu Y, Ding F, Zhang J. Chemical vapor deposition synthesis of near-zigzag single-walled carbon nanotubes with stable tube-catalyst interface. Science Advances. 2016;**2**(5):e1501729. DOI: 10.1126/sciadv.1501729

[7] Fagan JA, Haroz EH, Ihly R, Gui H, Blackburn JL, Simpson JR, et al. Isolation of >1 nm diameter single-wall carbon nanotube species using aqueous two-phase extraction. ACS Nano. 2015;**9**(5):5377-5390. DOI: 10.1021/acsnano.5b01123

[8] Green AA, Hersam MC. Nearly single-chirality single-walled carbon nanotubes produced via orthogonal iterative density gradient ultracentrifugation. Advanced Materials. 2011;**23**(19):2185-2190. DOI: 10.1002/adma.201100034

[9] Liu HP, Nishide D, Tanaka T, Kataura H. Large-scale single-chirality separation of single-wall carbon nanotubes by simple gel chromatography. Nature Communications. 2011;**2**:309. DOI: 10.1038/ncomms1313

[10] Tu XM, Manohar S, Jagota A, Zheng M. DNA sequence motifs for structure-specific recognition and separation of carbon nanotubes. Nature. 2009;**460**(7252):250-253. DOI: 10.1038/nature08116

[11] Yomogida Y, Tanaka T, Zhang MF, Yudasaka M, Wei XJ, Kataura H. Industrial-scale separation of high-purity single-chirality single-wall carbon nanotubes for biological imaging. Nature Communications. 2016;**7**:12056. DOI: 10.1038/ncomms12056

[12] Kharlamova MV. Electronic properties of pristine and modified single-walled carbon nanotubes. Physics-Uspekhi. 2013;**56**(11):1047-1073. DOI: 10.3367/UFNe.0183.201311a.1145

[13] Kharlamova MV. Advances in tailoring the electronic properties of single-walled carbon nanotubes. Progress in Materials Science. 2016;**77**:125-211. DOI: 10.1016/j.pmatsci.2015.09.001

[14] Smith BW, Monthioux M, Luzzi DE. Encapsulated C_{60} in carbon

nanotubes. Nature. 1998;**396**(6709): 323-324. DOI: 10.1038/24521

[15] Sloan J, Hammer J, Zwiefka-Sibley M, Green MLH. The opening and filling of single walled carbon nanotubes (SWTs). Chemical Communications. 1998;(3):347-348. DOI: 10.1039/A707632K

[16] Govindaraj A, Satishkumar BC, Nath M, Rao CNR. Metal nanowires and intercalated metal layers in single-walled carbon nanotube bundles. Chemistry of Materials. 2000;**12**(1): 202-205. DOI: 10.1021/cm990546o

[17] Tonkikh AA, Tsebro VI, Obraztsova EA, Suenaga K, Kataura H, Nasibulin AG, et al. Metallization of single-wall carbon nanotube thin films induced by gas phase iodination. Carbon. 2015;**94**:768-774. DOI: 10.1016/j.carbon.2015.07.062

[18] Borowiak-Palen E, Ruemmeli MH, Gemming T, Pichler T, Kalenczuk RJ, Silva SRP. Silver filled single-wall carbon nanotubes-synthesis, structural and electronic properties. Nanotechnology. 2006;**17**(9):2415-2419. DOI: 10.1088/0957-4484/17/9/058

[19] Corio P, Santos AP, Santos PS, Temperini MLA, Brar VW, Pimenta MA, et al. Characterization of single wall carbon nanotubes filled with silver and with chromium compounds. Chemical Physics Letters. 2004;**383**(5-6):475-480. DOI: 10.1016/j.cplett.2003.11.061

[20] Kharlamova MV, Niu JJ. Comparison of metallic silver and copper doping effects on single-walled carbon nanotubes. Applied Physics A. 2012;**109**(1):25-29. DOI: 10.1007/s00339-012-7091-3

[21] Kharlamova MV, Niu JJ. Donor doping of single-walled carbon nanotubes by filling of channels with silver. Journal of Experimental and Theoretical Physics. 2012;**115**(3):485-491. DOI: 10.1134/S1063776112080092

[22] Kharlamova MV, Niu JJ. New method of the directional modification of the electronic structure of single-walled carbon nanotubes by filling channels with metallic copper from a liquid phase. JETP Letters. 2012;**95**(6):314-319. DOI: 10.1134/S0021364012060057

[23] Fujimori T, Morelos-Gomez A, Zhu Z, Muramatsu H, Futamura R, Urita K, et al. Conducting linear chains of sulphur inside carbon nanotubes. Nature Communications. 2013;**4**:2162. DOI: 10.1038/ncomms3162

[24] Philp E, Sloan J, Kirkland AI, Meyer RR, Friedrichs S, Hutchison JL, et al. An encapsulated helical one-dimensional cobalt iodide nanostructure. Nature Materials. 2003;**2**(12):788-791. DOI: 10.1038/nmat1020

[25] Sloan J, Novotny MC, Bailey SR, Brown G, Xu C, Williams VC, et al. Two layer 4: 4 co-ordinated KI crystals grown within single walled carbon nanotubes. Chemical Physics Letters. 2000;**329**(1-2):61-65. DOI: 10.1016/S0009-2614(00)00998-2

[26] Sloan J, Kirkland AI, Hutchison JL, Green MLH. Integral atomic layer architectures of 1D crystals inserted into single walled carbon nanotubes. Chemical Communications. 2002;(13):1319-1332. DOI: 10.1039/B200537A

[27] Sloan J, Friedrichs S, Meyer RR, Kirkland AI, Hutchison JL, Green MLH. Structural changes induced in nanocrystals of binary compounds confined within single walled carbon nanotubes: A brief review. Inorganica Chimica Acta. 2002;**330**:1-12. DOI: 10.1016/S0020-1693(01)00774-5

[28] Sloan J, Grosvenor SJ, Friedrichs S, Kirkland AI, Hutchison JL, Green MLH.

A one-dimensional BaI_2 chain with five- and six-coordination, formed within a single-walled carbon nanotube. Angewandte Chemie International Edition. 2002;**41**(7):1156-1159. DOI: 10.1002/1521-3773(20020402)41:7<1156:AID-ANIE1156>3.0.CO;2-N

[29] Sloan J, Kirkland AI, Hutchison JL, Green MLH. Aspects of crystal growth within carbon nanotubes. Comptes Rendus Physique. 2003;**4**(9):1063-1074. DOI: 10.1016/S1631-0705(03)00102-6

[30] Carter R, Sloan J, Kirkland AI, Meyer RR, Lindan PJD, Lin G, et al. Correlation of structural and electronic properties in a new low-dimensional form of mercury telluride. Physical Review Letters. 2006;**96**(21):215501. DOI: 10.1103/PhysRevLett.96.215501

[31] Carter R, Suyetin M, Lister S, Dyson MA, Trewhitt H, Goel S, et al. Band gap expansion, shear inversion phase change behaviour and low-voltage induced crystal oscillation in low-dimensional tin selenide crystals. Dalton Transactions. 2014;**43**(20):7391-7399. DOI: 10.1039/C4DT00185K

[32] Kharlamova MV. Novel approach to tailoring the electronic properties of single-walled carbon nanotubes by the encapsulation of high-melting gallium selenide using a single-step process. JETP Letters. 2013;**98**(5):272-277. DOI: 10.1134/S0021364013180069

[33] Kharlamova MV. Comparative analysis of electronic properties of tin, gallium, and bismuth chalcogenide-filled single-walled carbon nanotubes. Journal of Materials Science. 2014;**49**(24):8402-8411. DOI: 10.1007/s10853-014-8550-3

[34] Yashina LV, Eliseev AA, Kharlamova MV, Volykhov AA, Egorov AV, Savilov SV, et al. Growth and characterization of one-dimensional SnTe crystals within the single-walled carbon nanotube channels. Journal of Physical Chemistry C. 2011;**115**(9):3578-3586. DOI: 10.1021/jp1107087

[35] Costa PMFJ, Sloan J, Rutherford T, Green MLH. Encapsulation of Re_xO_y clusters within single-walled carbon nanotubes and their in tubulo reduction and sintering to Re metal. Chemistry of Materials. 2005;**17**(26):6579-6582. DOI: 10.1021/cm0510209

[36] Hulman M, Kuzmany H, Costa PMFJ, Friedrichs S, Green MLH. Light-induced instability of PbO-filled single-wall carbon nanotubes. Applied Physics Letters. 2004;**85**(11):2068-2070. DOI: 10.1063/1.1790603

[37] Burteaux B, Claye A, Smith BW, Monthioux M, Luzzi DE, Fischer JE. Abundance of encapsulated C_{60} in single-wall carbon nanotubes. Chemical Physics Letters. 1999;**310**(1-2):21-24. DOI: 10.1016/S0009-2614(99)00720-4

[38] Chamberlain TW, Camenisch A, Champness NR, Briggs GAD, Benjamin SC, Ardavan A, et al. Toward controlled spacing in one-dimensional molecular chains: Alkyl-chain-functionalized fullerenes in carbon nanotubes. Journal of the American Chemical Society. 2007;**129**(27):8609-8614. DOI: 10.1021/ja071803q

[39] Gimenez-Lopez MD, Chuvilin A, Kaiser U, Khlobystov AN. Functionalised endohedral fullerenes in single-walled carbon nanotubes. Chemical Communications. 2011;**47**(7):2116-2118. DOI: 10.1039/C0CC02929G

[40] Kataura H, Maniwa Y, Kodama T, Kikuchi K, Hirahara K, Suenaga K, et al. High-yield fullerene encapsulation in single-wall carbon nanotubes. Synthetic Metals. 2001;**121**(1-3):1195-1196. DOI: 10.1016/S0379-6779(00)00707-4

[41] Suenaga K, Okazaki T, Wang CR, Bandow S, Shinohara H, Iijima S. Direct imaging of $Sc_2@C_{84}$ molecules

encapsulated inside single-wall carbon nanotubes by high resolution electron microscopy with atomic sensitivity. Physical Review Letters. 2003;**90**(5):055506. DOI: 10.1103/PhysRevLett.90.055506

[42] Guan LH, Shi ZJ, Li MX, Gu ZN. Ferrocene-filled single-walled carbon nanotubes. Carbon. 2005;**43**(13):2780-2785. DOI: 10.1016/j.carbon.2005.05.025

[43] Li LJ, Khlobystov AN, Wiltshire JG, Briggs GAD, Nicholas RJ. Diameter-selective encapsulation of metallocenes in single-walled carbon nanotubes. Nature Materials. 2005;**4**(6):481-485. DOI: 10.1038/nmat1396

[44] Shiozawa H, Pichler T, Gruneis A, Pfeiffer R, Kuzmany H, Liu Z, et al. A catalytic reaction inside a single-walled carbon nanotube. Advanced Materials. 2008;**20**(8):1443-1449. DOI: 10.1002/adma.200701466

[45] Kharlamova MV, Eliseev AA, Yashina LV, Lukashin AV, Tretyakov YD. Synthesis of nanocomposites on basis of single-walled carbon nanotubes intercalated by manganese halogenides. Journal of Physics Conference Series. 2012;**345**:012034. DOI: 10.1088/1742-6596/345/1/012034

[46] Kharlamova MV. Electronic properties of single-walled carbon nanotubes filled with manganese halogenides. Applied Physics A. 2016;**122**(9):791. DOI: 10.1007/s00339-016-0335-x

[47] Kharlamova MV, Brzhezinskaya MM, Vinogradov AS, Suzdalev IP, Maksimov YV, Imshennik VK, et al. The formation and properties of one-dimensional $FeHal_2$ (HaI=Cl, Br, I) nanocrystals in channels of single-walled carbon nanotubes. Nanotechnologies in Russia. 2009;**4**(9-10):634-646. DOI: 10.1134/S1995078009090080

[48] Kharlamova MV, Eliseev AA, Yashina LV, Petukhov DI, Liu CP, Wang CY, et al. Study of the electronic structure of single-walled carbon nanotubes filled with cobalt bromide. JETP Letters. 2010;**91**(4):196-200. DOI: 10.1134/S0021364010040089

[49] Kharlamova MV, Yashina LV, Eliseev AA, Volykhov AA, Neudachina VS, Brzhezinskaya MM, et al. Single-walled carbon nanotubes filled with nickel halogenides: Atomic structure and doping effect. Physica Status Solidi B. 2012;**249**(12):2328-2332. DOI: 10.1002/pssb.201200060

[50] Kharlamova MV. Raman spectroscopy study of the doping effect of the encapsulated iron, cobalt, and nickel bromides on single-walled carbon nanotubes. Journal of Spectroscopy. 2015;**2015**:653848. DOI: 10.1155/2015/653848

[51] Eliseev AA, Yashina LV, Verbitskiy NI, Brzhezinskaya MM, Kharlamova MV, Chernysheva MV, et al. Interaction between single walled carbon nanotube and 1D crystal in CuX@SWCNT (X = Cl, Br, I) nanostructures. Carbon. 2012;**50**(11):4021-4039. DOI: 10.1016/j.carbon.2012.04.046

[52] Fedotov PV, Tonkikh AA, Obraztsova EA, Nasibulin AG, Kauppinen EI, Chuvilin AL, et al. Optical properties of single-walled carbon nanotubes filled with CuCl by gas-phase technique. Physica Status Solidi B. 2014;**251**(12):2466-2470. DOI: 10.1002/pssb.201451240

[53] Chernysheva MV, Eliseev AA, Lukashin AV, Tretyakov YD, Savilov SV, Kiselev NA, et al. Filling of single-walled carbon nanotubes by CuI nanocrystals via capillary technique. Physica E: Low-dimensional Systems and Nanostructures. 2007;**37**(1-2):62-65. DOI: 10.1016/j.physe.2006.10.014

[54] Kumskov AS, Zhigalina VG, Chuvilin AL, Verbitskiy NI, Ryabenko AG, Zaytsev DD, et al. The structure of 1D and 3D CuI nanocrystals grown within 1.5-2.5 nm single wall carbon nanotubes obtained by catalyzed chemical vapor deposition. Carbon. 2012;**50**(12):4696-4704. DOI: 10.1016/j.carbon.2012.05.061

[55] Kharlamova MV, Yashina LV, Volykhov AA, Niu JJ, Neudachina VS, Brzhezinskaya MM, et al. Acceptor doping of single-walled carbon nanotubes by encapsulation of zinc halogenides. European Physical Journal B. 2012;**85**(1):34. DOI: 10.1140/epjb/e2011-20457-6

[56] Kharlamova MV. Comparison of influence of incorporated 3d-, 4d-and 4f-metal chlorides on electronic properties of single-walled carbon nanotubes. Applied Physics A. 2013;**111**(3):725-731. DOI: 10.1007/s00339-013-7639-x

[57] Falaleev NS, Kumskov AS, Zhigalina VG, Verbitskiy II, Vasiliev AL, Makarova AA, et al. Capsulate structure effect on SWNTs doping in $Rb_xAg_{1-x}I$@SWNT composites. CrystEngComm. 2017;**19**(22):3063-3070. DOI: 10.1039/C7CE00155J

[58] Eliseev AA, Yashina LV, Brzhezinskaya MM, Chernysheva MV, Kharlamova MV, Verbitsky NI, et al. Structure and electronic properties of AgX (X = Cl, Br, I)-intercalated single-walled carbon nanotubes. Carbon. 2010;**48**(10):2708-2721. DOI: 10.1016/j.carbon.2010.02.037

[59] Kharlamova MV, Kramberger C, Mittelberger A, Yanagi K, Pichler T, Eder D. Silver chloride encapsulation-induced modifications of Raman modes of metallicity-sorted semiconducting single-walled carbon nanotubes. Journal of Spectroscopy. 2018;**2018**:5987428. DOI: 10.1155/2018/5987428

[60] Kharlamova MV, Kramberger C, Domanov O, Mittelberger A, Yanagi K, Pichler T, et al. Fermi level engineering of metallicity-sorted metallic single-walled carbon nanotubes by encapsulation of few-atom-thick crystals of silver chloride. Journal of Materials Science. 2018;**53**(18):13018-13029. DOI: 10.1007/s10853-018-2575-y

[61] Kharlamova MV, Kramberger C, Domanov O, Mittelberger A, Saito T, Yanagi K, et al. Comparison of doping levels of single-walled carbon nanotubes synthesized by arc-discharge and chemical vapor deposition methods by encapsulated silver chloride. Physica Status Solidi B. 2018;**255**(12):1800178. DOI: 10.1002/pssb.201800178

[62] Kharlamova MV, Yashina LV, Lukashin AV. Charge transfer in single-walled carbon nanotubes filled with cadmium halogenides. Journal of Materials Science. 2013;**48**(24):8412-8419. DOI: 10.1007/s10853-013-7653-6

[63] Kharlamova MV, Kramberger C, Pichler T. Semiconducting response in single-walled carbon nanotubes filled with cadmium chloride. Physica Status Solidi B. 2016;**253**(12):2433-2439. DOI: 10.1002/pssb.201600300

[64] Zakalyukin RM, Mavrin BN, Dem'yanets LN, Kiselev NA. Synthesis and characterization of single-walled carbon nanotubes filled with the superionic material SnF_2. Carbon. 2008;**46**(12):1574-1578. DOI: 10.1016/j.carbon.2008.06.055

[65] Kharlamova MV. Rare-earth metal halogenide encapsulation-induced modifications in Raman spectra of single-walled carbon nanotubes. Applied Physics A. 2015;**118**(1):27-35. DOI: 10.1007/s00339-014-8880-7

[66] Kharlamova MV, Kramberger C, Mittelberger A. Raman spectroscopy study of the doping effect of the encapsulated terbium halogenides

on single-walled carbon nanotubes. Applied Physics A. 2017;**123**(4):239. DOI: 10.1007/s00339-017-0873-x

[67] Kharlamova MV, Volykhov AA, Yashina LV, Egorov AV, Lukashin AV. Experimental and theoretical studies on the electronic properties of praseodymium chloride-filled single-walled carbon nanotubes. Journal of Materials Science. 2015;**50**(16):5419-5430. DOI: 10.1007/s10853-015-9086-x

[68] Ayala P, Kitaura R, Nakanishi R, Shiozawa H, Ogawa D, Hoffmann P, et al. Templating rare-earth hybridization via ultrahigh vacuum annealing of $ErCl_3$ nanowires inside carbon nanotubes. Physical Review B. 2011;**83**(8):085407. DOI: 10.1103/PhysRevB.83.085407

[69] Kharlamova MV, Yashina LV, Lukashin AV. Comparison of modification of electronic properties of single-walled carbon nanotubes filled with metal halogenide, chalcogenide, and pure metal. Applied Physics A. 2013;**112**(2):297-304. DOI: 10.1007/s00339-013-7808-y

[70] Fedoseeva YV, Orekhov AS, Chekhova GN, Koroteev VO, Kanygin MA, Seovskiy BV, et al. Single-walled carbon nanotube reactor for redox transformation of mercury dichloride. ACS Nano. 2017;**11**(9):8643-8649. DOI: 10.1021/acsnano.7b04361

[71] Dresselhaus MS, Dresselhaus G, Jorio A, Souza AG, Saito R. Raman spectroscopy on isolated single wall carbon nanotubes. Carbon. 2002;**40**(12):2043-2061. DOI: 10.1016/S0008-6223(02)00066-0

[72] Araujo PT, Maciel IO, Pesce PBC, Pimenta MA, Doorn SK, Qian H, et al. Nature of the constant factor in the relation between radial breathing mode frequency and tube diameter for single-wall carbon nanotubes. Physical Review B. 2008;**77**(24):241403R. DOI: 10.1103/PhysRevB.77.241403

[73] Fouquet M, Telg H, Maultzsch J, Wu Y, Chandra B, Hone J, et al. Longitudinal optical phonons in metallic and semiconducting carbon nanotubes. Physical Review Letters. 2009;**102**(7):075501. DOI: 10.1103/PhysRevLett.102.075501

[74] Brown SDM, Corio P, Marucci A, Dresselhaus MS, Pimenta MA, Kneipp K. Anti-stokes Raman spectra of single-walled carbon nanotubes. Physical Review B. 2000;**61**(8):R5137-R5140. DOI: 10.1103/PhysRevB.61.R5137

[75] Jorio A, Souza AG, Dresselhaus G, Dresselhaus MS, Swan AK, Unlu MS, et al. G-band resonant Raman study of 62 isolated single-wall carbon nanotubes. Physical Review B. 2002;**65**(15):155412. DOI: 10.1103/PhysRevB.65.155412

[76] Briones A, Liu XJ, Kramberger C, Saito T, Pichler T. Nanochemical reactions by laser annealing of ferrocene filled single-walled carbon nanotubes. Physica Status Solidi B. 2011;**248**(11):2488-2491. DOI: 10.1002/pssb.201100114

[77] Kharlamova MV, Sauer M, Saito T, Krause S, Liu X, Yanagi K, et al. Inner tube growth properties and electronic structure of ferrocene-filled large diameter single-walled carbon nanotubes. Physica Status Solidi B. 2013;**250**(12):2575-2580. DOI: 10.1002/pssb.201300089

[78] Kharlamova MV, Kramberger C, Saito T, Shiozawa H, Pichler T. In situ Raman spectroscopy studies on time-dependent inner tube growth in ferrocene-filled large diameter single-walled carbon nanotubes. Physica Status Solidi B. 2014;**251**(12):2394-2400. DOI: 10.1002/pssb.201451166

[79] Liu XJ, Kuzmany H, Saito T, Pichler T. Temperature dependence of inner tube growth from ferrocene-filled single-walled carbon nanotubes. Physica

Status Solidi B. 2011;**248**(11):2492-2495. DOI: 10.1002/pssb.201100116

[80] Sauer M, Shiozawa H, Ayala P, Ruiz-Soria G, Kataura H, Yanagi K, et al. In situ filling of metallic single-walled carbon nanotubes with ferrocene molecules. Physica Status Solidi B. 2012;**249**(12):2408-2411. DOI: 10.1002/pssb.201200127

[81] Shiozawa H, Pichler T, Pfeiffer R, Kuzmany H, Kataura H. Ferrocene encapsulated in single-wall carbon nanotubes: A precursor to secondary tubes. Physica Status Solidi B. 2007;**244**(11):4102-4105. DOI: 10.1002/pssb.200776137

[82] Shiozawa H, Pichler T, Kramberger C, Gruneis A, Knupfer M, Buchner B, et al. Fine tuning the charge transfer in carbon nanotubes via the interconversion of encapsulated molecules. Physical Review B. 2008;**77**(15):153402. DOI: 10.1103/PhysRevB.77.153402

[83] Kocsis D, Kaptas D, Botos A, Pekker A, Kamaras K. Ferrocene encapsulation in carbon nanotubes: Various methods of filling and investigation. Physica Status Solidi B. 2011;**248**(11):2512-2515. DOI: 10.1002/pssb.201100160

[84] Liu XJ, Kuzmany H, Ayala P, Calvaresi M, Zerbetto F, Pichler T. Selective enhancement of photoluminescence in filled single-walled carbon nanotubes. Advanced Functional Materials. 2012;**22**(15):3202-3208. DOI: 10.1002/adfm.201200224

[85] Plank W, Pfeiffer R, Schaman C, Kuzmany H, Calvaresi M, Zerbetto F, et al. Electronic structure of carbon nanotubes with ultrahigh curvature. ACS Nano. 2010;**4**(8):4515-4522. DOI: 10.1021/nn100615d

[86] Sauer M, Shiozawa H, Ayala P, Ruiz-Soria G, Liu XJ, Chernov A, et al. Internal charge transfer in metallicity sorted ferrocene filled carbon nanotube hybrids. Carbon. 2013;**59**:237-245. DOI: 10.1016/j.carbon.2013.03.014

[87] Kharlamova MV, Kramberger C, Saito T, Shiozawa H, Pichler T. Growth dynamics of inner tubes inside cobaltocene-filled single-walled carbon nanotubes. Applied Physics A. 2016;**122**(8):749. DOI: 10.1007/s00339-016-0282-6

[88] Kharlamova MV, Kramberger C, Sato Y, Saito T, Suenaga K, Pichler T, et al. Chiral vector and metal catalyst-dependent growth kinetics of single-wall carbon nanotubes. Carbon. 2018;**133**:283-292. DOI: 10.1016/j.carbon.2018.03.046

[89] Kharlamova MV, Sauer M, Saito T, Sato Y, Suenaga K, Pichler T, et al. Doping of single-walled carbon nanotubes controlled via chemical transformation of encapsulated nickelocene. Nanoscale. 2015;**7**(4):1383-1391. DOI: 10.1039/C4NR05586A

[90] Kharlamova MV, Sauer M, Egorov A, Kramberger C, Saito T, Pichler T, et al. Temperature-dependent inner tube growth and electronic structure of nickelocene-filled single-walled carbon nanotubes. Physica Status Solidi B. 2015;**252**(11):2485-2490. DOI: 10.1002/pssb.201552206

[91] Kharlamova MV, Kramberger C, Saito T, Sato Y, Suenaga K, Pichler T, et al. Chirality-dependent growth of single-wall carbon nanotubes as revealed inside nano-test tubes. Nanoscale. 2017;**9**(23):7998-8006. DOI: 10.1039/C7NR01846K

[92] Kharlamova MV, Kramberger C, Sauer M, Yanagi K, Saito T, Pichler T. Inner tube growth and electronic properties of metallicity-sorted nickelocene-filled semiconducting single-walled carbon nanotubes. Applied Physics A. 2018;**124**(3):247. DOI: 10.1007/s00339-018-1679-1

[93] Shiozawa H, Pichler T, Kramberger C, Rummeli M, Batchelor D, Liu Z, et al. Screening the missing electron: Nanochemistry in action. Physical Review Letters. 2009;**102**(4):046804. DOI: 10.1103/PhysRevLett.102.046804

[94] Shiozawa H, Kramberger C, Rummeli M, Batchelor D, Kataura H, Pichler T, et al. Electronic properties of single-walled carbon nanotubes encapsulating a cerium organometallic compound. Physica Status Solidi B. 2009;**246**(11-12):2626-2630. DOI: 10.1002/pssb.200982344

[95] Shiozawa H, Giusca CE, Silva SRP, Kataura H, Pichler T. Capillary filling of single-walled carbon nanotubes with ferrocene in an organic solvent. Physica Status Solidi B. 2008;**245**(10):1983-1985. DOI: 10.1002/pssb.200879626